Journal of Materials Chemistry C

Accepted Manuscript

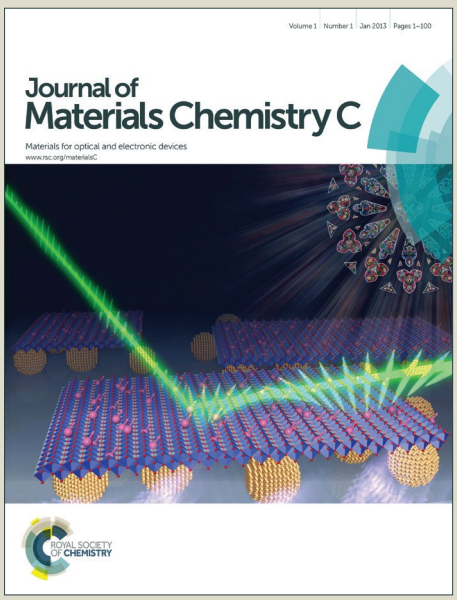

ROYAL SOCIETY OF CHEMISTRY

www.rsc.org/materialsC

Journal Name

RSCPublishing

ARTICLE

Carbon dioxide sensor based on a surface acoustic wave device with a graphene/nickel/L-alanine multilayer film

Cite this: DOI: 10.1039/x0xx00000x

Received ooth January 2012,
Accepted ooth January 2012

DOI: 10.1039/x0xx00000x

www.rsc.org/

Sheng Xu,[a] Cuiping Li,[b] Hongji Li,[c] Mingji Li,*[b] Changqing Qu,[b] and Baohe Yang*[ab]

Surface acoustic wave (SAW) sensors for carbon dioxide (CO_2) detection containing graphene/nickel (Ni)/L-alanine composite sensing films were investigated. ST-cut quartz SAW resonators were modified with L-alanine, Ni nanoparticles and graphene by electrodeposition. The presence of graphene markedly enhanced the CO_2 sensing properties of the sensor. The performance of the sensor containing a graphene/Ni/L-alanine composite film depended both on the pH of the solution used to deposit the L-alanine sensitive layer and operation temperature. The CO_2 sensing mechanism of the SAW sensor is based on the adsorption of CO_2 and H_2O gas molecules by graphene, the catalytic reaction of Ni nanoparticles, and the reaction between L-alanine and CO_2 gas molecules; that is, the three materials in the sensitive layer have a synergistic effect. From analysis of changes in acoustic signals, exposure of the sensor to CO_2 not only changed the conductivity of the film but also produced a additional capacitance, which ultimately changed the equivalent capacitance of the sensor.

1. Introduction

Carbon dioxide (CO_2) is present in Earth's atmosphere at concentrations close to 397.82 ppm.[1] As the primary greenhouse gas emitted through human activities, the atmospheric concentration of CO_2 has increased approximately 30% since preindustrial times, which plays a critical role in climate change.[2, 3] Concern about climate change has greatly stimulated research on the detection, capture and storage of CO_2.[2, 4, 5] CO_2 sensors are used for environmental monitoring of greenhouse gases, health care, indoor air-quality control, and fire detection systems. Various types of CO_2 sensors have been developed including solid electrolyte,[6] capacitive, resistive,[7, 8] optical [9-12] and surface acoustic wave (SAW) sensors.[13, 14]

Recently, SAW gas sensors have attracted substantial attention because of their advantages of high sensitivity, speed, and accuracy, as well as good reliability, and low cost.[14, 15] The core component of a SAW gas sensor is the sensing film. This sensitive membrane that serves as the feedback element of an oscillator circuit is deposited on the acoustic propagation path of each SAW device. A change in the conductivity of the sensitive film causes a frequency shift of the SAW device.[16] In gases, the conductivity of the sensitive layer is directly affected by gas concentration. Acoustoelectric coupling of the travelling electric potential wave associated with the SAW with charge carriers in the film decreases the velocity of the acoustic wave, altering the oscillation frequency of the circuit. Among different types of sensing films available, polymer,[7, 17-19] dye,[16] carbon nanotube,[13, 20, 21] and semiconductor films[15, 22] have mostly been used in gas sensors because of their high sensitivity and selectivity, and fast response time to changes in gas/vapor atmospheres. Electrochemical deposition is a simple, efficient, and inexpensive method to deposit various materials as a gas-sensitive layer for sensors containing SAW devices.[17, 23, 24]

Graphene is a monolayer of carbon atoms packed to form a two-dimensional 2D honeycomb lattice.[25-27] The large surface area and unique properties of graphene, including its sensitivity to single absorbed molecules, mean that it lends itself to integration with SAW devices, although relatively little work on this topic has been reported to date.[28] Thalmeier *et al*.[29] and Zhang *et al*.[30] both made theoretically studied the change in SAW propagation on a piezoelectric substrate caused by interaction with charge carriers in graphene. Acoustic charge transport, which exploits this piezoelectric interaction, has been reported from graphene transferred onto piezoelectric substrates.[31, 32] Nash and co-workers investigated the effects of argon and air loading on quartz SAW devices, which have the advantage of greater temperature stability than other substrates, with and without graphene in the acoustic path.[28] Nash *et al*. studied the acoustoelectric charge transport in graphene, and found that the acoustoelectric current was proportional to both

the SAW intensity and the attenuation of the wave caused by charge transport.[33] In addition, Nash *et al*. investigated the temperature dependence of the acoustoelectric current in graphene. At high SAW frequencies, the acoustoelectric current decreases with decreasing temperature.[34] Xuan *et al.* reported ZnO/glass SAW humidity sensors with a graphene oxide sensing layer that have high sensitivity and fast response.[35] However, little research on the SAW propagation, interaction and sensing ability of graphene structures has been reported.

Amino acid molecules are zwitterions, and the pH of their solution determines whether the form of the amino acid is the zwitterion, anion, or cation.[36] In addition, altering the pH of a solution is a way to control crystal polymorph; larger needle-like crystals at pH 3.1–4.5, mesocrystals at pH 7.5, short tubes at pH 8.0 and needle-like crystals at pH 9.2.[37] Alanine has the chemical formula $CH_3CH(NH_2)COOH$ and can selectively adsorb CO_2 gas.[38, 39] The main structural change in alanine is conversion of the positively charged $–NH_3^+$ group to a neutral $–NH_2$ group; the carboxylate moiety $–CO_2^-$ remains unchanged in structure and charge.[40] Recently, gas sensors based on porous NiO nanostructures have been fabricated by layering NiO nanomaterials on interdigital transducer (IDT) electrodes.[41]

In this work, we use graphene, alanine and Ni nanoparticles to develop a CO_2 gas SAW sensor. The sensor contains a graphene/Ni/$_L$-alanine sensing layer fabricated by electrochemical deposition and oscillator circuits were not used. We investigate the selectivity, sensitivity, reversibility and chemical characteristics of this sensor at room temperature.

2. Experimental

2.1. Fabrication of the graphene/Ni/$_L$-alanine/SAW sensor

A single-port SAW resonator was fabricated on ST-cut quartz (3.45×0.90×0.37 mm) with the SAW propagation direction perpendicular to the crystallographic x-axis (90°-rotated) and an acoustic velocity of 3,158 m s^{-1}. Each sensor consisted of an IDT containing 171 pairs of electrodes (1.8 μm) with a pitch of 3.6 μm and two reflector banks each containing 309 electrodes, and acoustic aperture (*W*) of 144 μm. The central frequency of the SAW resonators was approximately 434.1544 MHz.

Electrochemical deposition of the sensitive layer was performed in a conventional three-electrode cell consisting of a SAW resonator as the working electrode, a platinum sheet as the counter electrode, and an Ag/AgCl electrode as the reference electrode (Fig. 1a). The SAW resonators were treated by potential scanning between 0.2 and 1.2 V at 100 mV s^{-1} for 30 cycles in 0.1 M Phosphate buffer solutions (PBSs) at various pH containing 0.01 mol L^{-1} $_L$-alanine. PBSs with pH ranging from 4.0 to 10.0 were prepared by mixing stock solutions of 0.1 M NaH_2PO_4 and 0.1 M Na_2HPO_4, and the pH was adjusted with H_3PO_4 (1 mol L^{-1}) and NaOH (1 mol L^{-1}) solutions. The SAW resonators were then rinsed with ethanol and water to give the $_L$-alanine-modified SAW ($_L$-alanine/SAW) sensor. Electrodeposition of Ni nanoparticles onto the $_L$-alanine/SAW sensor was carried out in a solution of Na_2SO_4 and $NiSO_4$ (both 0.1 mol L^{-1}) by potential cycling between -0.6 and 0.6 V (*vs*. Ag/AgCl) at a scan rate of 100 mV s^{-1} for 30 cycles. Finally, the electrodeposition of graphene was performed in a solution of 0.4 mg mL^{-1} graphene and 0.1 M PBS (pH 7.0) at 1.5 V for 5 min in a two-electrode cell. The sensor was rinsed with ultrapure water and dried under N_2 gas. Graphene oxide was prepared from natural graphite using a modified Hummers method,[42] and reduced graphene oxide (hereafter referred to as graphene) was produced *via* chemical vapor deposition.[43]

2.2. Characterization

The sensor was characterized by field-emission scanning electron microscopy (FE-SEM; JEOL JSM-6700F, Japan), transmission electron microscopy (TEM; JEOL, JEM-2100, Japan), Raman spectroscopy (Thermo Scientific, DXR, USA) and atomic force microscopy (AFM; Agilent 5500, USA).

2.3. Gas sensing measurements

The detection platform of the SAW gas sensor is shown in Fig. 1b. The SAW sensor was placed in the test chamber with a volume of 180 mL facing the gas inlet. The total gas flow rate was maintained at 500 mL min^{-1} by a mass flow meter. Before gas sensing, the sensing SAW device was preheated to 200 °C for 1 h to remove any gas absorbed on the sensitive membrane surface, which may interfere with the subsequent gas sensing. The SAW sensor was placed in an N_2 environment for 1 h to equilibrate. A blend of CO_2 and air/or N_2 gas was delivered to the gas chamber for different periods, followed by desorption of CO_2 by purging the system with high-purity N_2 gas to recover the center frequency of the SAW sensor. The frequency resonance was tested by a network analyzer (E5070B, Agilent ENA, USA).

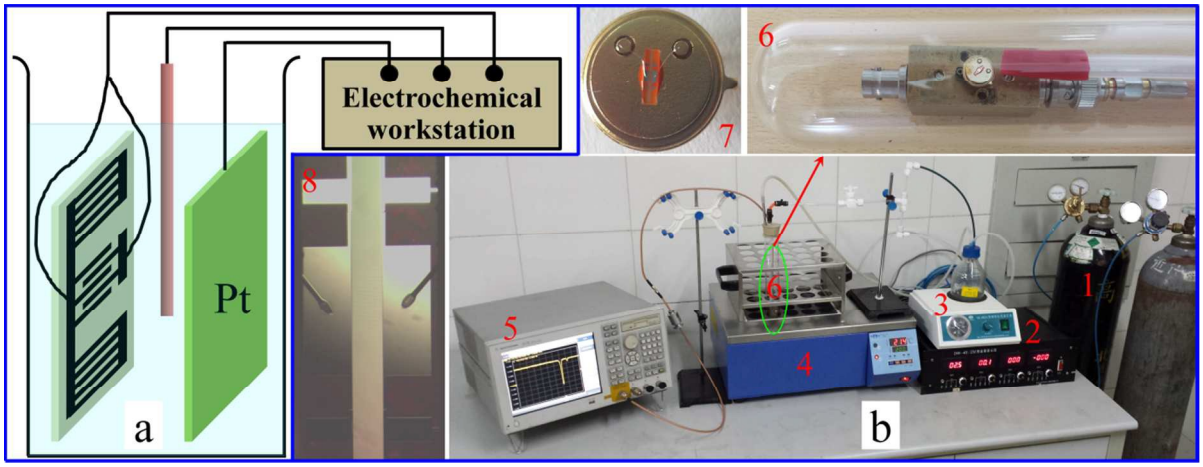

Fig. 1 (a) Schematic diagram of electrodeposition system. (b) Structure of detecting platform using the SAW device. (1) Cylinder. (2) Gas flow control system. (3) Vacuum pump. (4) Heating system. (5) Network analyzer. (6) Test chamber. The SAW sensor was positioned inside the quartz chamber to face the gas inlet. (7) SAW sensor. The SAW sensor was plugged into the test shielding box. (8) IDT electrodes of SAW device.

When a SAW sensor is exposed to the target gas, its electrical and mechanical characteristics change according to the absorption capacity of the active sensing region, resulting in a frequency shift.[44] Considering the effects of perturbation by mass loading including elastic and electric loading, the propagation characteristics of the surface wave are affected as follows:[15, 20]

$$\frac{\Delta f}{f_0} = \frac{\Delta v}{v_0} = -c_m f_0 \Delta\rho_s + c_e f_0 h \Delta\left[\frac{(4\mu / v_0^2(\eta + \mu)}{\eta + 2\mu}\right] - \left[\frac{K^2}{2}\right]\Delta\left[\frac{\sigma_s^2}{\sigma_s^2 + v_0^2 C_S'^2}\right] \quad (1)$$

where v_0 is unperturbed wave velocity, c_m and c_e are the sensitivity coefficients for mass and elasticity, ρ_s is the mass per area, μ and η are the shear and bulk moduli of the film, σ_s is the sheet conductivity of the film, C_s' is the capacitance per length of the SAW substrate material, and f_0 is the center frequency of the SAW device. In the case of a sensor with a three-layer sensitive membrane, C'_S is the sum of the capacitance of the sensitive layers and static capacitance for the IDT. Therefore, the sensitivity for CO_2 gas is mainly related to the response of the sensitive membrane layer, which not only changes the film conductivity, but also produces a additional capacitance (the capacitance of the sensitive layer), which ultimately changes C'_S. Such a signal generation mechanism is distinctly different those of previously reported sensors, which are generally based on changes in the electrical conductivity of sensors under the influence of gas molecules.[45]

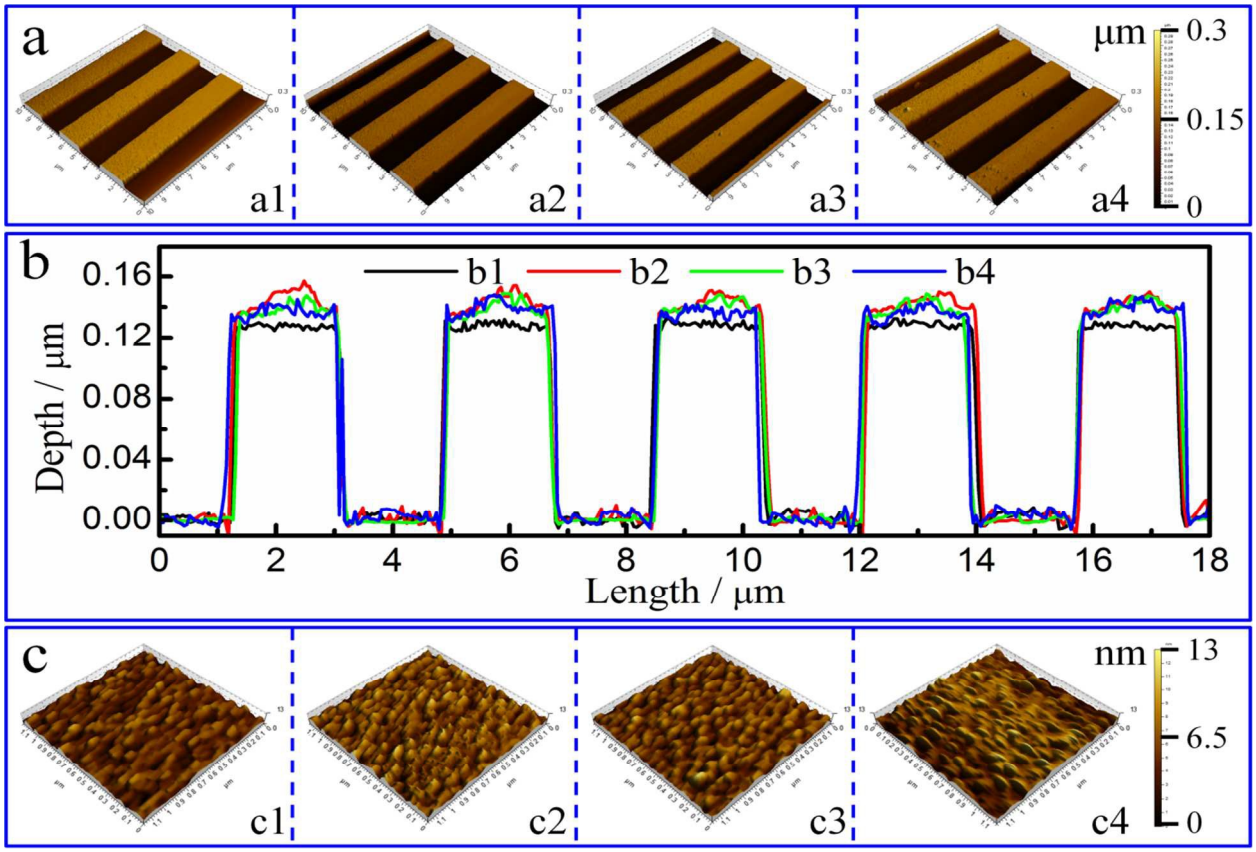

Fig. 2 (a) Three-dimensional AFM images and (b) line profiles of the bare SAW (a1, b1), $_L$-alanine/SAW (a2, b2), Ni/$_L$-alanine/SAW (a3, b3), and graphene/Ni/$_L$-alanine/SAW (a4, b4) devices. (c) AFM images of the bare electrode (c1), $_L$-alanine layer on the IDT electrode surface (c2), Ni layer on the $_L$-alanine/IDT surface (c3), and graphene layer on the Ni/$_L$-alanine/IDT surface (c4).

3. Results and discussion

Fig. 2 shows three-dimensional AFM images and line profiles of the SAW devices with various sensitive membranes. The average surface roughness of the IDT electrode and substrate was estimated from the AFM images, as well as its dependence on the type of modified sensitive membrane. The modified SAW devices possessed coarser microstructure than the pristine one. The measured root-mean-square (RMS) roughness of the IDT electrodes on bare SAW, $_L$-alanine/SAW, Ni/$_L$-alanine/SAW, and graphene/Ni/$_L$-alanine/SAW devices was 1.46, 1.59, 1.58, and 1.88 nm, respectively. Obviously, the RMS values were markedly larger than that of the bare IDT electrode after modification with a sensitive membrane. The thickness of the IDT and substrate roughness also changed (Fig. 2b), indicating that each of the sensitive layers was successfully deposited onto the SAW devices.

Fig. 3a shows SEM images of IDT electrodes of bare SAW, $_L$-alanine/SAW, Ni/$_L$-alanine/SAW and graphene/Ni/$_L$-alanine/SAW devices. The SEM image of the graphene/Ni/$_L$-alanine/SAW device reveals dots on the device surface, which could be aggregates of graphene sheets. Fig. 3b shows a TEM image and Raman spectrum of graphene, and SEM image of the IDT electrode on the graphene/Ni/$_L$-alanine/SAW device at higher resolution than the images in Fig. 3a. The TEM image of graphene shows the graphene sheets are flake-like and transparent, indicating that we successfully prepared high-quality graphene sheets, consistent with a previous report.[46] The Raman spectrum of graphene is dominated by a G band at 1,572.7 cm^{-1}, D band at 1,343.2 cm^{-1}, and 2D band at 2,700.8 cm^{-1}. The D band is induced by local defects and disorder, and has been previously observed along the edges of graphene and graphite. For graphene, the 2D peak is a single sharp peak, while that of graphite consists of two peaks, D_1 and D_2.[26] Elemental mapping in scanning SEM mode and the corresponding energy-dispersive X-ray spectroscopy (EDS) mapping in Fig. 3c indicates the presence of Al, N, Ni, C, Si and O elements in the graphene/Ni/$_L$-alanine/SAW device. In this structure, Al originates from the IDT electrode, Si and O from the piezoelectric film, N from $_L$-alanine, Ni from the catalyst layer, and C from $_L$-alanine and graphene. These maps confirm that the IDT electrode and substrate were completely covered with a highly uniform graphene/Ni/$_L$-alanine sensitive layer.

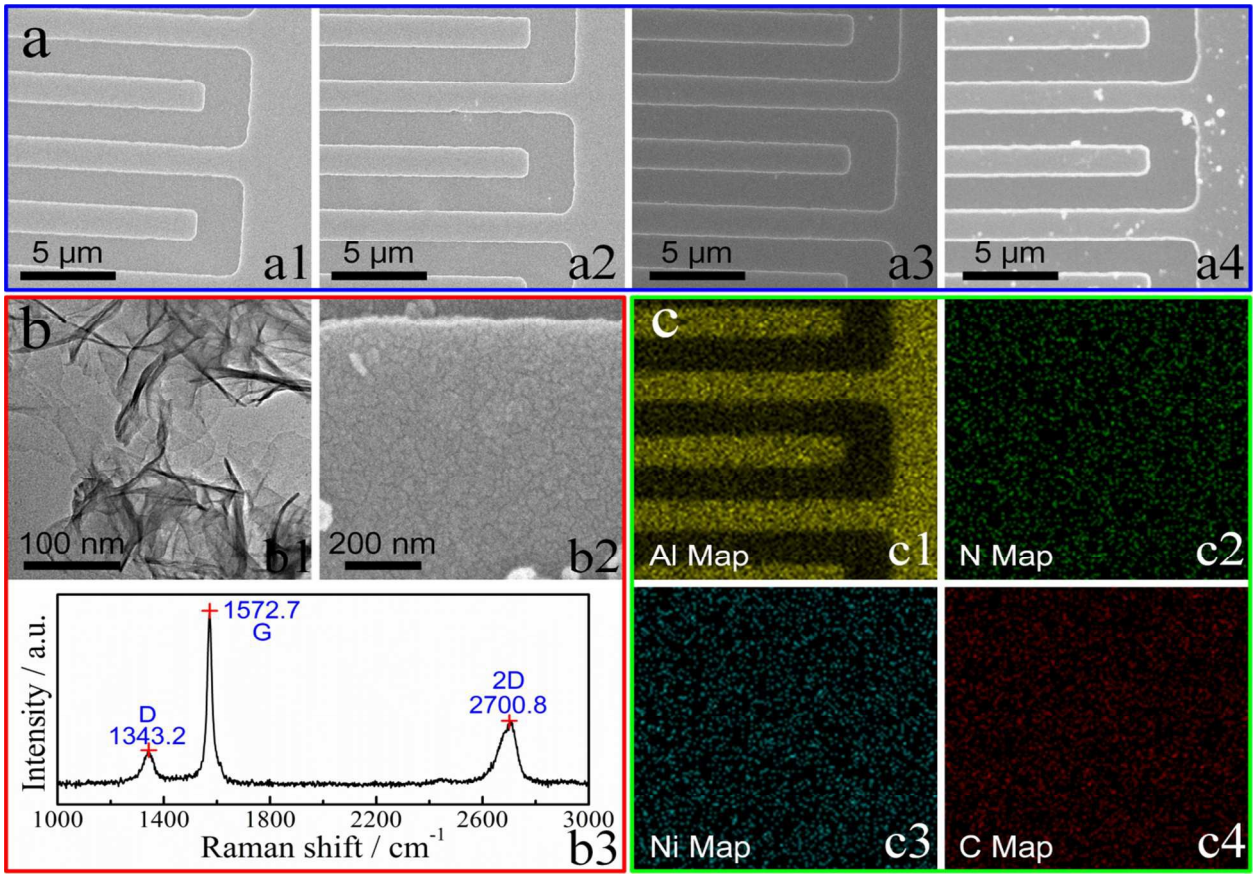

Fig. 3 (a) SEM images of IDT electrodes on bare SAW (a1), $_L$-alanine/SAW (a2), Ni/$_L$-alanine/SAW (a3), and graphene/Ni/$_L$-alanine/SAW devices (a4). (b) TEM image (b1) and high-resolution SEM image (b2), and Raman spectrum of graphene (b3) of the graphene/Ni/$_L$-alanine/IDT electrode. (c) EDS element mapping of Al, N, Ni and C for the Ni/$_L$-alanine/graphene/SAW device.

Fig. 4 shows the frequency responses of bare SAW, $_L$-alanine/SAW, Ni/$_L$-alanine/SAW, graphene/$_L$-alanine/SAW and graphene/Ni/$_L$-alanine/SAW devices in air and CO_2 at room temperature. After $_L$-alanine was electrodeposited onto the SAW device, a negative shift in frequency was observed. A positive frequency shift was found after electrodeposition of Ni, and the frequency shifted from positive to negative appeared after deposition of graphene. For the bare SAW device, the curves measured in air and CO_2 overlapped, so this device is unsuitable for sensing purposes. The frequency of the graphene/Ni/$_L$-alanine/SAW structure was higher in CO_2 than in air. The inset of Fig. 4 shows that the frequency shift for the graphene/Ni/$_L$-alanine/SAW device between air and CO_2 is larger than those of the other structures. Therefore, the graphene/Ni/$_L$-alanine/SAW device is the best suited for CO_2 sensing of the devices examined here. The resonant frequency (f) of SAW devices can be correlated to the effective SAW velocity (v_e) and the wavelength (λ) or pitch (p) of the device using the following relationship:

$$f = v_e / \lambda = v_e / 2p \quad (2)$$

Theoretically, λ does not change, so the frequency response is related to v_e. The perturbations in v_e may be expressed as:[47, 48]

$$v_e = v_f + \Delta v_e + \Delta v_M \quad (3)$$

where v_f is the free-surface velocity, Δv_e is the change in velocity caused by electrical loading, and Δv_M is the change in velocity caused by mechanical loading. $_L$-Alanine is insulating so its acoustoelectric interaction is neglected. For the IDT electrode modified with an $_L$-alanine layer, the mass loading effect dominated the frequency response, causing the observed negative frequency shift.[49] Ni nanoparticles and graphene nanosheets are conductive materials, so both the acoustoelectric interaction and mass loading effect are considered. When the device is modified with both Ni and graphene layers, the metallization ratio (η=IDT width (a)/p) will be affected, as shown in Fig. 2b.

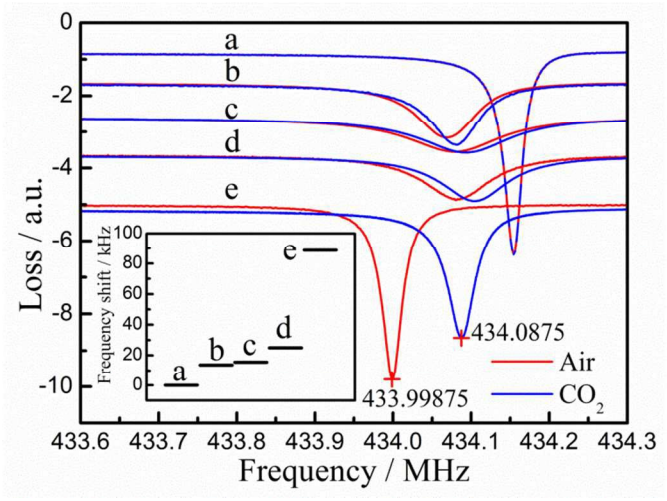

Fig. 4 Frequency characteristics of (a) bare SAW, (b) $_L$-alanine/SAW, (c) Ni/$_L$-alanine/SAW, (d) graphene/$_L$-alanine/SAW and (e) graphene/Ni/$_L$-alanine/SAW devices in air (red curves) and CO_2 (blue curves) at room temperature. The inset show the frequency shift between CO_2 and air for the devices.

Fig. 5 shows the frequency response curves of the graphene/Ni/$_L$-alanine/SAW sensor in air and CO_2 at temperatures of 25 to 200 °C and pH of 4 to 10. Figure 6a shows the corresponding dependence of frequency response on temperature at various pH. The solution pH value has an important influence on frequency response. Under air and CO_2, a very clear frequency shift depending on temperature was observed in the range of 25–200 °C. The thermal stability of the frequency of the graphene/Ni/$_L$-alanine/SAW sensor is characterized by its temperature coefficient of frequency (TCF), which is defined as the relative change in frequency with temperature and is usually expressed in ppm K^{-1}.[50]

$$TCF = \frac{1}{f}\frac{df}{dT} \quad (4)$$

f [graphene/Ni/$_L$-alanine/SAW] = (434.006±0.007)–(5.1×10^{-4}±0.5×10^{-4}) T (5)

f [bare SAW] = (434.18±0.01)–(7.02×10^{-4}±0.7×10^{-4}) T (6)

Equations 5 and 6 show the functional relationship between the frequency of the SAW sensors and experimental temperature, which is plotted in Fig. 6b. TCF of the graphene/Ni/$_L$-alanine/SAW sensor in air is -1.22 ppm K^{-1}, which is higher than -1.61 ppm K^{-1} of the bare SAW device, showing that the composite device has higher thermal stability than the bare one. This is advantageous to improve the sensitivity of the sensor. In addition, the frequency response of the graphene/Ni/$_L$-alanine/SAW sensor containing $_L$-alanine layers deposited at different pH was investigated. As the pH was increased from 4.0 to 7.0 during deposition of $_L$-alanine, the center frequency of the SAW sensor shifted to more negative value. Conversely, with increasing pH from 7.0 to 10.0, the center frequency of the SAW sensor shifted to more positive value. For the Ni-graphene/$_L$-alanine/SAW sensor, the maximum frequency shift for CO_2 gas is observed at pH 10.0 and 200 °C (Fig. 6a). Taking into account the stability and sensitivity of this sensor, we selected conditions of 0.1 M PBS at pH 10.0 and 200 °C for subsequent experiments.

Graphene has high intrinsic electrical conductivity, large specific surface area, and high chemical stability, so graphene layers can readily capture gas molecules such as CO_2 and H_2O.[8, 51-53] In the electrodeposition of graphene, the Ni nanoparticles act as nuclear sites and a reducing agent, and the oxygen-containing groups on graphene can form strong bonds with Ni. In addition, Ni nanoparticles may also catalyze the hydrolysis of CO_2, which would enhance the selectivity of this sensor. $_L$-Alanine molecules can be stabilized in different forms, as shown in Fig. 7. Between pH 4.5 and 7.5, $_L$-alanine is almost fully zwitterionic (d). Below pH 1.5, more than 90% of molecules are in the cationic form (c), whereas above pH 11, more than 90% of $_L$-alanine molecules in aqueous solution are anionic (d):[54]

$$CH_3CH(NH_2)COO^-+H^+ \rightleftharpoons CH_3CH(NH_3^+)COO^- \quad (7)$$

$$CH_3CH(NH_2)COOH+H^+ \rightleftharpoons CH_3CH(NH_3^+)COOH \quad (8)$$

$$CH_3CH(NH_2)COOH+OH^- \rightleftharpoons CH_3CH(NH_2)COO^- +H_2O \quad (9)$$

$_L$-Alanine is bonded to the metal IDT electrodes and piezoelectric film surface by either the N atom or the O atoms of the carboxylate group (-COOH).[38] Under basic conditions (pH 10), the reactions between CO_2 and the various types of $_L$-alanine in the SAW sensor are as follows:

$$[CH_3CH(NH_2)COO\text{--SAW}]+CO_2+H_2O \rightleftharpoons [CH_3CH(NH_2)COOH\text{-SAW}]+HCO_3^- \rightleftharpoons [CH_3CH(NH_3^+)COOH\text{-SAW}]+2CO_3^{2-} \quad (10)$$

$$[CH_3CH(NH_3^+\text{-SAW})COO^-]+CO_2+H_2O \rightleftharpoons [CH_3CH(NH_3^+\text{-SAW})COOH]+HCO_3^- \quad (11)$$

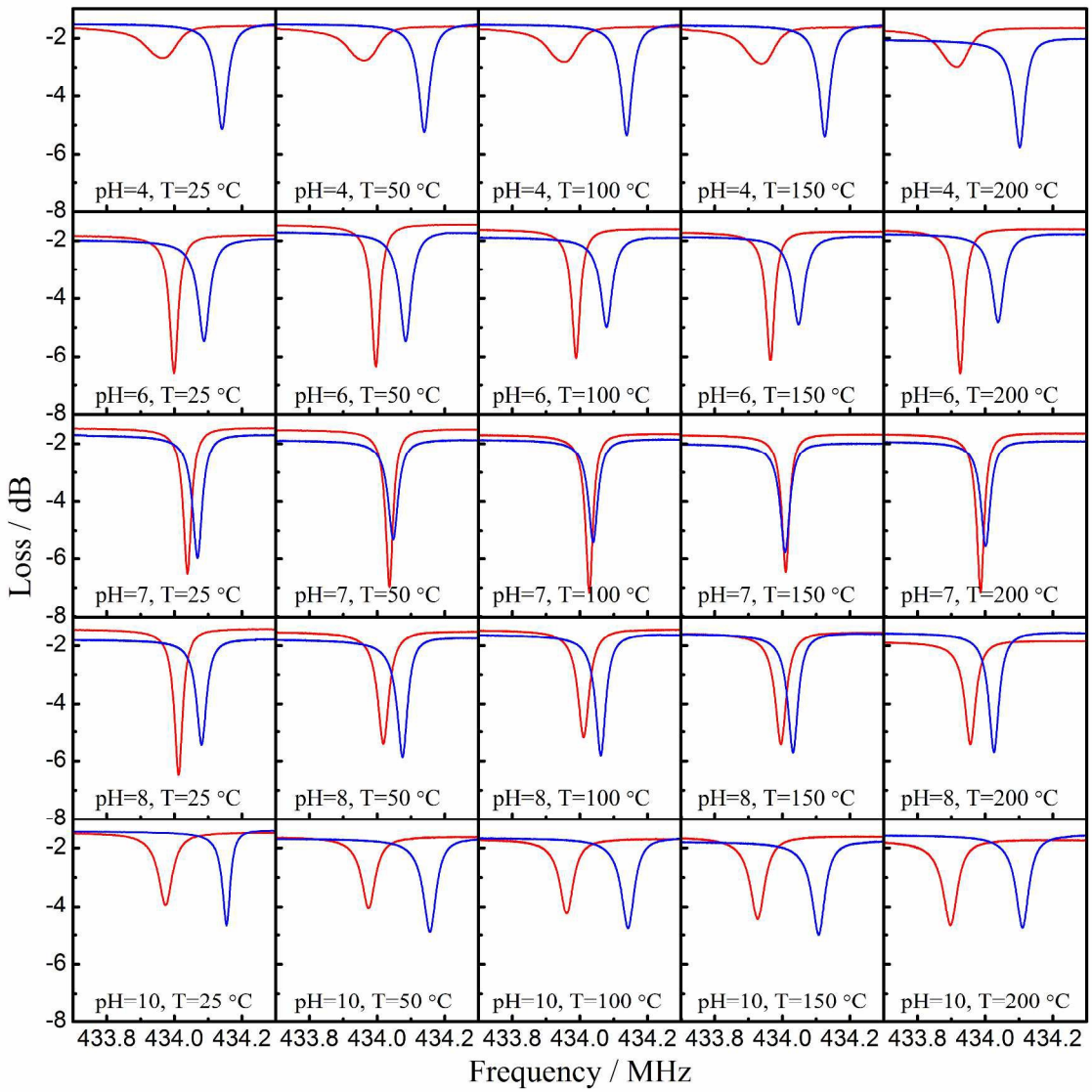

Fig. 5 Frequency response curves of the graphene/Ni/$_{L}$-alanine/SAW sensor in air (red) and CO_2 (blue) at temperatures of 25–200 °C and pH of 4–10.

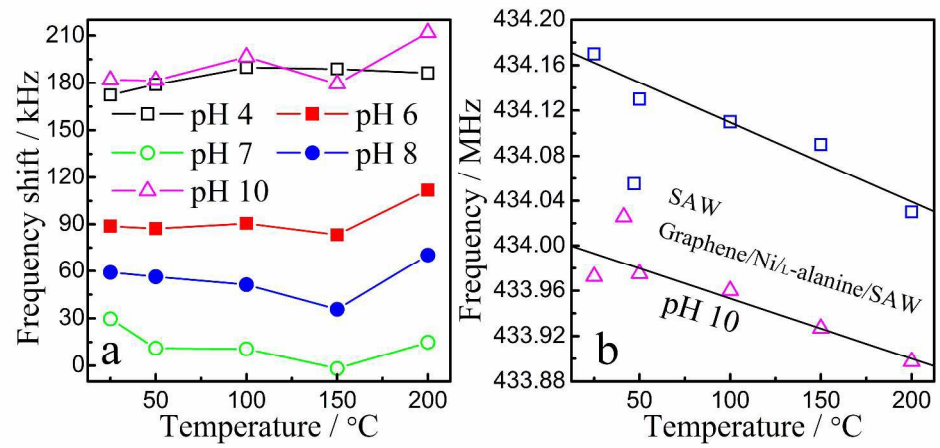

Fig. 6 (a) Frequency shift of the graphene/Ni/L-alanine/SAW sensor as a function of temperature with L-alanine layers deposited at various pH values. (b) Linear decrease of frequency with increasing temperature for the graphene/Ni/L-alanine/SAW sensor in air.

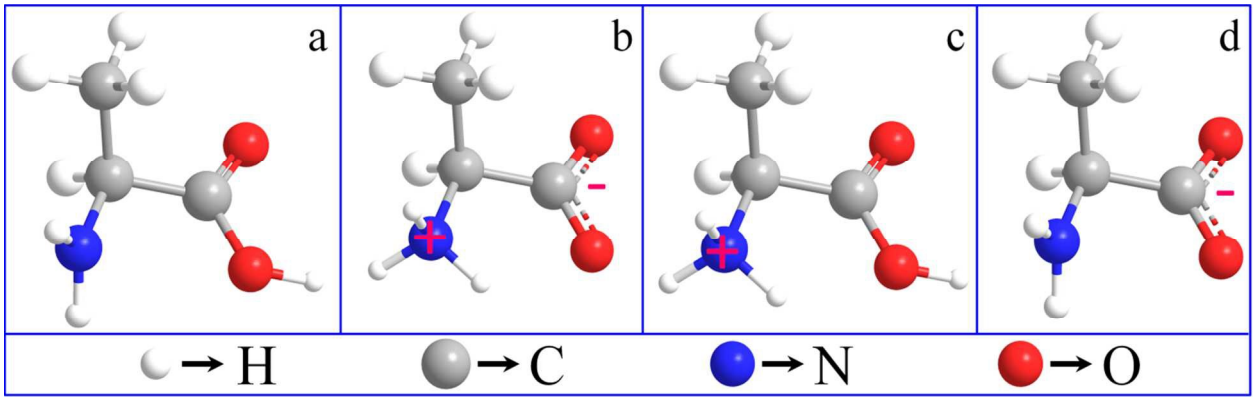

Fig. 7 Interaction of L-alanine with CO_2 at different pH. (a) Nonionic, (b) zwitterionic, (c) cationic, and (d) anionic. Red, oxygen; blue, nitrogen; dark gray, carbon; light gray, hydrogen.

Fig. 8 illustrates the response of the graphene/Ni/L-alanine/SAW sensor to different concentrations of CO_2 gas at 200 °C. We assumed here that the response and recovery times corresponded to the times when the sensor output reached 90% of the final value and 10% above the baseline value, respectively. The evaluation of the response of the sensor was carried out for different periods. The sensor was exposed to CO_2 for 60 s each time and then purged with air. For almost all concentrations of CO_2, the sensor recovered in less than 20 s to 50% of its initial signal and in 50 s to >90% of its initial signal. In addition, the reproducibility of the Ni-graphene/ L-alanine/SAW sensor was further investigated for 4–7 exposure cycles. The exposure cycles measured for each concentration exhibited very similar curves. The fluctuation of frequency shift was less than 10%, and the response and recovery times were similar for the consecutive tests, indicating the results were reliable and the sensor shows good reproducibility.

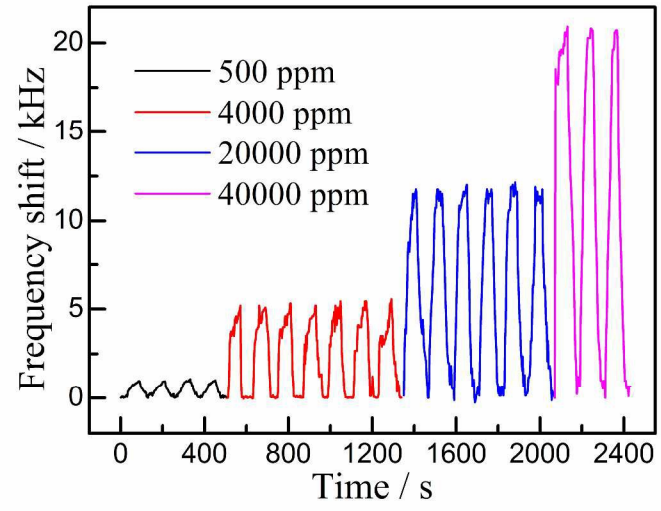

Fig. 8 Dynamic response of the graphene/Ni/L-alanine/SAW sensor towards different concentrations of CO_2 gas at 200 °C.

Fig. 9 shows the frequency shifts of the graphene/Ni/L-alanine/SAW sensor as a function of CO_2 concentration. The response of the sensor increased rapidly with increasing CO_2 concentration in the range from 0 to 38,500 ppm. When the CO_2 concentration was increased from 0 to 2,000 ppm and 2,000 to 38,500 ppm, the responses showed almost linear increases with slopes of 2.07 and 0.377 Hz ppm^{-1}, respectively. A frequency shift of 667 Hz was obtained at a low concentration of CO_2 gas of 200 ppm, while a frequency shift of 4,200 Hz was observed for a CO_2 concentration of 2,000 ppm. The sensitivity for CO_2 concentration was measured as 2.51 MHz ppm^{-1} m^{-2} (0 to 2,000 ppm) and 0.46 MHz ppm^{-1} m^{-2} (2,000 to 38,500 ppm). The detection limit of the sensor could reach 200 ppm.

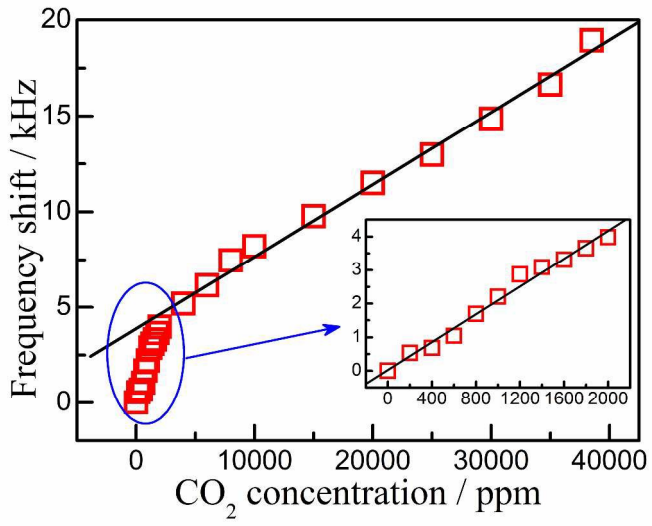

Fig. 9 Response of the sensor to different concentrations of CO_2 gas at 200 °C.

For CO_2 gas, the baseline shift of the sensor was low and could be neglected as shown in Fig. 10. The sensor did not have a marked response to 500 ppm air, Ar, O_2 or ethanol (C_2H_5OH) gases, showing frequency shifts of approximately 0.9, 0.2, 0.15 and 225 kHz, respectively. Although the interference of ethanol is relatively large, these results suggest that the sensor has strong selectivity for CO_2.

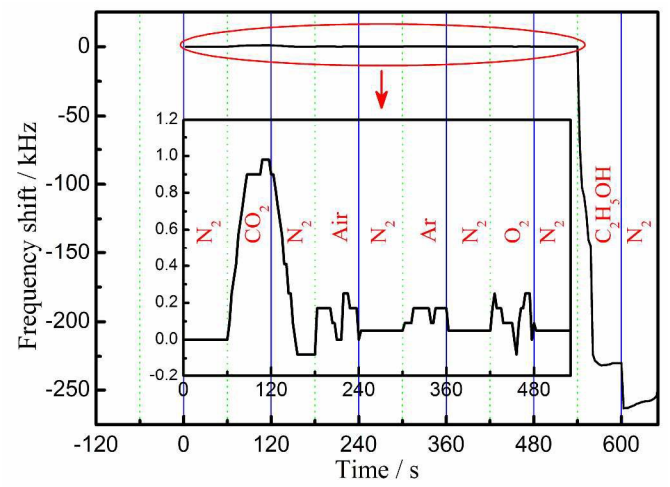

Fig. 10 Dynamic frequency shifts of the graphene/Ni/$_L$-alanine/SAW sensor to 500 ppm CO_2, air, Ar, O_2 and ethanol gases.

4. Conclusions

SAW sensors coated with graphene/Ni/$_L$-alanine composite films to detect CO_2 were developed. The sensor containing the composite film exhibited the roughest surface morphology and best sensing properties of the devices examined. This sensor showed a positive frequency shift of 667 Hz to CO_2 at a concentration of 200 ppm, as well as excellent selectivity, stability and reproducibility. By comparing the responses of sensors containing an $_L$-alanine film and graphene/Ni/$_L$-alanine composite, the presence of Ni nanoparticles and graphene nanosheets was found to enhance the sensitivity of the sensor because of their ability to promote the adsorption of gas and catalytic reactions.

Acknowledgements

The authors gratefully acknowledge financial support from the Hi-tech Research and Development Program of China (863) (No. 2013AA030801), the Natural Science Foundation of Tianjin (No. 13JCZDJC36000), the National Natural Science Foundation of China (Nos. 61301045, and 61401306), and the Excellent Young Teachers Program of Tianjin.

Notes and references

[a] School of Precision Instrument and Optoelectronics Engineering, Tianjin University, Tianjin 300072, P. R. China
[b] Tianjin Key Laboratory of Film Electronic and Communication Devices, School of Electronics Information Engineering, Tianjin University of Technology, Tianjin 300384, P. R. China
[c] Tianjin Key Laboratory of Organic Solar Cells and Photochemical Conversion, School of Chemistry & Chemical Engineering, Tianjin University of Technology, Tianjin 300384, P.R. China.

† Electronic Supplementary Information (ESI) available: [details of any supplementary information available should be included here]. See DOI: 10.1039/b000000x/

1 S. Fanget, S. Hentz, P. Puget, J. Arcamone, M. Matheron, E. Colinet, P. Andreucci, L. Duraffourg, E. Myers and M. L. Roukes, *Sens. Actuators B: Chem*, 2011, 160, 804-821.
2 K. Fan, H. Qin, L. Wang, L. Ju and J. Hu, *Sens. Actuators B: Chem*, 2013, 177, 265-269.
3 C. Finn, S. Schnittger, L. J. Yellowlees and J. B. Love, *Chem. Commun.*, 2012, 48, 1392-1399.
4 C. Van Leeuwen, A. Hensen and H. A. J. Meijer, *Int. J. Greenh. Gas Control*, 2013, 19, 420-431.
5 V. Lates, A. Falch, A. Jordaan, R. Peach and R. J. Kriek, *Electrochim. Acta*, 2014, 128, 75-84.
6 J. Yoon, G. Hunter, S. Akbar and P. K. Dutta, *Sens. Actuators B: Chem*, 2013, 182, 95-103.
7 C. J. Chiang, K. T. Tsai, Y. H. Lee, H. W. Lin, Y. L. Yang, C. C. Shih, C. Y. Lin, H. A. Jeng, Y. H. Weng, Y. Y. Cheng, K. C. Ho and C. A. Dai, *Microelectron. Eng.*, 2013, 111, 409-415.
8 S. Muhammad Hafiz, R. Ritikos, T. J. Whitcher, N. Md. Razib, D. C. S. Bien, N. Chanlek, H. Nakajima, T. Saisopa, P. Songsiriritthigul, N. M. Huang and S. A. Rahman, *Sens. Actuators B: Chem*, 2014, 193, 692-700.
9 Y. Ma, H. Xu, Y. Zeng, C.-L. Ho, C.-H. Chui, Q. Zhao, W. Huang and W.-Y. Wong, *J. Mater. Chem. C*, 2015, 3, 66-72.
10 S. M. Borisov, R. Seifner and I. Klimant, *Anal. Bioanal. Chem.*, 2011, 400, 2463-2474.
11 S. Schutting, S. M. Borisov and I. Klimant, *Anal. Chem.*, 2013, 85, 3271-3279.
12 Y. Zilberman, S. K. Ameri and S. R. Sonkusale, *Sens. Actuators B: Chem*, 2014, 194, 404-409.
13 S. Sivaramakrishnan, R. Rajamani, C. S. Smith, K. A. McGee, K. R. Mann and N. Yamashita, *Sens. Actuators B: Chem*, 2008, 132, 296-304.
14 C. Lim, W. Wang, S. Yang and K. Lee, *Sens. Actuators B: Chem*, 2011, 154, 9-16.
15 Y. L. Tang, Z. J. Li, J. Y. Ma, H. Q. Su, Y. J. Guo, L. Wang, B. Du, J. J. Chen, W. L. Zhou, Q. K. Yu and X. T. Zu, *J. Hazard. Mater.*, 2014, 280, 127-133.
16 A. J. Ricco, S. J. Martin and T. E. Zipperian, *Sens. Actuators*, 1985, 8, 319-333.
17 D. Matatagui, M. J. Fernandez, J. P. Santos, J. Fontecha, I. Sayago, M. C. Horrillo, I. Gracia and C. Cane, *J. Nanomater.*, 2014, 243037, 1-8.
18 I. Sayago, M. J. Fernández, J. L. Fontecha, M. C. Horrillo, C. Vera, I. Obieta and I. Bustero, *Sens. Actuators B: Chem*, 2011, 156, 1-5.
19 D. Y. Gallimore, P. J. Millard and M. Pereira da Cunha, *Acs Appl Mater Inter*, 1998, 1, 2382-2389.
20 I. Sayago, M. J. Fernandez, J. L. Fontecha, M. C. Horrillo, C. Vera, I. Obieta and I. Bustero, *Sens. Actuators B: Chem*, 2012, 175, 67-72.
21 M. David, M. Arab, C. Martino, L. Delmas, F. Guinneton and J. R. Gavarri, *Thin Solid Films*, 2012, 520, 4786-4791.
22 H. Oh, K. J. Lee, J. Baek, S. S. Yang and K. Lee, *Microelectron. Eng.*, 2013, 111, 154-159.
23 L. Zhang, J. Zhang and C. Zhang, *Biosens. Bioelectron.*, 2009, 24, 2085-2090.
24 S. Xu, M. Li, Y. Zhu, L. Wang, P. Yang and P. K. Chu, *Electrochim. Acta*, 2014, 132, 165-171.
25 R. Arsat, M. Breedon, M. Shafiei, P. G. Spizziri, S. Gilje, R. B. Kaner, K. Kalantar-Zadeh and W. Wlodarski, *Chem. Phys. Lett.*, 2009, 467, 344-347.
26 A. C. Ferrari, J. C. Meyer, V. Scardaci, C. Casiraghi, M. Lazzeri, F. Mauri, S. Piscanec, D. Jiang, K. S. Novoselov, S. Roth and A. K. Geim, *Phys. Rev. Lett.*, 2006, 97, 187401.
27 K. S. Novoselov, A. K. Geim, S. V. Morozov, D. Jiang, Y. Zhang, S. V. Dubonos, I. V. Grigorieva and A. A. Firsov, *Science*, 2004, 306, 666-669.
28 E. F. Whitehead, E. M. Chick, L. Bandhu, L. M. Lawton and G. R. Nash, *Appl. Phys. Lett.*, 2013, 103, 063110.
29 P. Thalmeier, B. Dora and K. Ziegler, *Phys. Rev. B*, 2010, 81, 041409.
30 S. H. Zhang and W. Xu, *AIP Adv.*, 2011, 1, 022146.
31 V. Miseikis, J. E. Cunningham, K. Saeed, R. O'Rorke and A. G. Davies, *Appl. Phys. Lett.*, 2012, 100, 133105.

32 P. V. Santos, T. Schumann, M. H. Oliveira, J. M. J. Lopes and H. Riechert, *Appl. Phys. Lett.*, 2013, 102, 221907
33 L. Bandhu, L. M. Lawton and G. R. Nash, *Appl. Phys. Lett.*, 2013, 103, 133101.
34 L. Bandhu and G. R. Nash, *Appl. Phys. Lett.*, 2014, 105, 263106.
35 W. Xuan, M. He, N. Meng, X. He, W. Wang, J. Chen, T. Shi, T. Hasan, Z. Xu, Y. Xu and J. K. Luo, *Sci. Rep.*, 2014, 4, 1-9.
36 J. Li, X. G. Wang, M. T. Klein and T. B. Brill, *Int. J. Chem. Kinet.*, 2002, 34, 271-277.
37 Y. R. Ma, H. Colfen and M. Antonietti, *J. Phys. Chem. B*, 2006, 110, 10822-10828.
38 A. P. Sandoval, J. M. Orts, A. Rodes and J. M. Feliu, *Electrochim. Acta*, 2013, 89, 72-83.
39 U. E. Aronu, H. F. Svendsen and K. A. Hoff, *Int. J. Greenh. Gas Control*, 2010, 4, 771-775.
40 S. Ma, T. B. Freedman, X. Cao and L. A. Nafie, *J. Mol. Struct.*, 2006, 799, 226-238.
41 J. Wang, L. M. Wei, L. Y. Zhang, C. H. Jiang, E. S. W. Kong and Y. F. Zhang, *J. Mater. Chem.*, 2012, 22, 8327-8335.
42 W. S. Hummers and R. E. Offeman, *J. Am. Chem. Soc.*, 1958, 80, 1339-1339.
43 M. Li, W. Guo, H. Li, S. Xu, C. Qu and B. Yang, *Appl. Surf. Sci.*, 2014, 317, 1100-1106.
44 H. C. Hao, K. T. Tang, P. H. Ku, J. S. Chao, C. H. Li, C. M. Yang and D. J. Yao, *Sens. Actuators B: Chem*, 2010, 146, 545-553.
45 W. Jakubik, *Sens. Actuators B: Chem*, 2014, 203, 511-516.
46 M. F. El-Kady, V. Strong, S. Dubin and R. B. Kaner, *Science*, 2012, 335, 1326-1330.
47 W. P. Jakubik, *Thin Solid Films*, 2011, 520, 986-993.
48 K. Blotekjaer, K. A. Ingebrigtsen and H. Skeie, *IEEE Trans. Electron Devices*, 1973, ED-20, 1133-1138.
49 C.-Y. Shen, C.-P. Huang and W.-T. Huang, *Sens. Actuators B: Chem*, 2004, 101, 1-7.
50 X. L. He, D. J. Li, J. Zhou, W. B. Wang, W. P. Xuan, S. R. Dong, H. Jin and J. K. Luo, *J. Mater. Chem. C*, 2013, 1, 6210-6215.
51 V. Chandra, S. U. Yu, S. H. Kim, Y. S. Yoon, D. Y. Kim, A. H. Kwon, M. Meyyappan and K. S. Kim, *Chem. Commun.*, 2012, 48, 735-737.
52 A. K. Mishra and S. Ramaprabhu, *AIP Adv.*, 2011, 1, 032152.
53 D. Zhou, Q.-Y. Cheng, Y. Cui, T. Wang, X. Li and B.-H. Han, *Carbon*, 2014, 66, 592-598.
54 A. R. Garcia, R. B. de Barros, J. P. Lourenco and L. M. Ilharco, *J. Phys. Chem. A*, 2008, 112, 8280-8287.